Journal of Materials Science: Materials in Electronics (2018) 29:5282–5286
https://doi.org/10.1007/s10854-017-8492-z

$Ln_3Al_5O_{12}:Mn^{4+}$ (Ln = Y and Lu): non-rare-earth doped red phosphor for improving light properties of white light emitting diodes

Zheng-Wei Yu[1] · Xiao-Yu Sun[1] · Zhen-Qing Wang[1]

Received: 14 November 2017 / Accepted: 27 December 2017 / Published online: 2 January 2018

Abstract
We fabricated a series of $Y_3Al_5O_{12}:Mn^{4+}$ and $Y_{1-y}Lu_yAl_5O_{12}:Mn^{4+}$ phosphors by a solid state reaction. The phase and the optical properties of the synthesized phosphors were investigated. Under the excitation at 465 nm, $Y_3Al_5O_{12}:Mn^{4+}$ phosphors show emission bands locating at deep red regions, which is induced by the spin- and parity-forbidden $^2E_g \rightarrow {}^4A_{1g}$ transitions of Mn^{4+}. The substitution of Y^{3+} by Lu^{3+} decreases the lattice parameter and thus strengthens the crystal field strength, which gives rise to the blue shift of emission band for $Y_{1-y}Lu_yAl_5O_{12}:Mn^{4+}$ phosphors. Due to the compensation of red light by $Y_3Al_5O_{12}:Mn^{4+}$ or $Y_{1-y}Lu_yAl_5O_{12}:Mn^{4+}$ phosphor, the values of correlated-color-temperature for fabricated LEDs are decreased, which leads to the suitable application for them in indoor illumination.

1 Introduction

The well known two drawbacks of the white light emitting diodes generated by the blue chip and $Y_3Al_5O_{12}:Ce^{3+}$ phosphors are the high correlated-color-temperature (CCT) and poor color-rendering index (CRI) [1, 2]. And these two drawbacks are mainly induced by the absence of red spectral contribution. To improve the light properties of white light emitting diodes, one of widely used methods is to mix a highly efficient red phosphor showing strong blue absorption with $Y_3Al_5O_{12}:Ce^{3+}$ yellow phosphor [3–8]. In past years, most of attempts for the red phosphors always focus on rare earth ions doped phosphors. But we know that the storage of rare earth elements are lacking. As a result, researchers try their best to look for elements with abundant storage those can be used in red phosphors. And in recent years, Mn^{4+} is found to be a good candidate because that Mn^{4+} activated red phosphors are much cheaper and possess desirable spectral features [7].

Over the last several years, Mn^{4+} doped aluminate garnet ($Ln_3Al_5O_{12}$, Ln = Lu, Y, Gd) phosphors have been paid more and more attentions [8–10]. It is known that Mn^{4+} prefers to occupy octahedral site to obtain high luminescence efficiency. In $Ln_3Al_5O_{12}$ hosts, Mn^{4+} priors to substitute octahedral Al^{3+} site due to the little distinction of radius between Al^{3+} (0.535 Å) and Mn^{4+} (0.530 Å), which gives large opportunities for $Ln_3Al_5O_{12}:Mn^{4+}$ phosphors to maintain the rigid garnet structure, decrease defect formation and guarantee the high luminescence efficiency of Mn^{4+} [8]. In this work, we synthesized a series of $Ln_3Al_5O_{12}:Mn^{4+}$ (Ln = Y and Lu) phosphors by the solid state reaction and investigated the luminescent properties of the synthesized phosphors.

2 Materials and method

A series of $Y_3Al_5O_{12}:x\%molMn^{4+}$ (x = 0.1, 0.2, 0.3 and 0.4) and $Y_{1-y}Lu_yAl_5O_{12}:0.3\%molMn^{4+}$ (y = 1, 2 and 3) phosphors were synthesized by a solid state reaction. The chemical reagents of Y_2O_3 (99.9%), Lu_2O_3 (99.9%), Al_2O_3 (99.9%) and MnO_2 (99.99%) were used as raw materials in the synthesis of $Ln_3Al_5O_{12}:Mn^{4+}$ (Ln = Y and Lu) phosphors. In the synthesis, chemical reagents with stoichiometric ratio were weighted and mixed in an agate mortar with the addition of a little amount of ethyl alcohol. After a thorough blending, the mixture was transferred into a platinum crucible and calcined at 1500 °C for 6 h in a muffle furnace. After the system cooled to room temperature naturally, the product was ground for subsequent measurements.

The phase was confirmed by X-ray powder diffraction (XRD) technique in a D8 advance X-ray diffractometer (Bruker, German) using Cu Kα radiation (λ = 0.15418 nm).

✉ Xiao-Yu Sun
xiaoyusun09@yeah.net

[1] College of Aerospace and Civil Engineering, Harbin Engineering University, Harbin 150001, China

The ultraviolet–visible (UV–vis) absorption spectra of the phosphors were recorded on a Cary 5000 UV–vis spectrophotometer. The excitation and emission spectra were measured by an Edinburgh Instrument FLS920 spectrophotometer equipped with a 150 W xenon lamp as the excitation source. The emission spectra of the fabricated LEDs were measured by a PMS-80 LED spectrophotocolorimeter.

3 Results and discussion

Figure 1 presents the XRD patterns of the synthesized $Y_3Al_5O_{12}$:0.3mol%Mn^{4+}, $Y_2LuAl_5O_{12}$:0.3mol%Mn^{4+}, $YLu_2Al_5O_{12}$:0.3mol%Mn^{4+}, $Lu_3Al_5O_{12}$:0.3mol%Mn^{4+} phosphors and the standard data of $Y_3Al_5O_{12}$ (JCPDs card no. 88-2047) and $Lu_3Al_5O_{12}$ (JCPDs card no. 73-1369). The ionic radius of Y^{3+} (1.019 Å) is larger that of Lu^{3+} (0.977 Å), which induces the decrease of lattice parameter with the increase of Lu^{3+} and the shifts of diffraction peaks to larger 2θ angles. In the XRD patterns of the synthesized phosphors, there are no diffraction peaks corresponding to other phase, suggesting that Lu^{3+} and Mn^{4+} have entirely incorporated into the structure of $Y_3Al_5O_{12}$. Herein, Lu^{3+} and Mn^{4+}, respectively, substitute Y^{3+} and Al^{3+} sites due to the similar ionic radii.

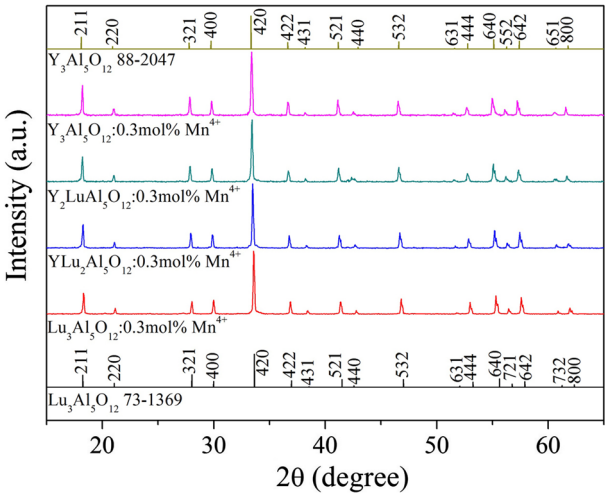

Fig. 1 XRD patterns of $Y_{1-y}Lu_yAl_5O_{12}$:0.3%molMn^{4+} (y = 0, 1, 2 and 3) phosphors and the standard XRD data of $Y_3Al_5O_{12}$ and $Lu_3Al_5O_{12}$

The luminescence of a phosphor has close relation with the crystal structure information of the host. Both $Y_3Al_5O_{12}$ and $Lu_3Al_5O_{12}$ have the cubic phase and belong to the space group of $Ia\bar{3}d(230)$. The parameters for $Y_3Al_5O_{12}$ and $Lu_3Al_5O_{12}$ are a = b = c = 12.008 Å and a = b = c = 11.906 Å, respectively. Figure 2 shows the crystal structures of $Y_3Al_5O_{12}$ and $Lu_3Al_5O_{12}$ of the 1 × 1 × 1 unit cell. In $Ln_3Al_5O_{12}$ (Ln = Y and Lu), Ln^{3+} ions coordinate with 8 O^{2-} ions and form the polyhedral shape, but Al^{3+} ions have two different lattice sites and coordinate with 6 and 4 O^{2-} ions to form AlO_6 octahedral and AlO_4 tetrahedral shapes. The AlO_6 octahedral and AlO_4 tetrahedral shapes connect with each other by means of sharing the same O^{2-} ion. And in $Y_3Al_5O_{12}$ and $Lu_3Al_5O_{12}$, the bond lengths between Mn and ligand O are 1.921 and 1.864 Å, respectively. As the atom number per cell keeps constant, the decrease of lattice parameter means the shortening of distance between atoms. This weakens the Mn interaction between atoms. So, Mn^{4+} will experience a stronger crystal field as the content of Lu increases.

Figure 3 shows the absorption spectra of $Y_3Al_5O_{12}$:x%molMn^{4+} (x = 0.1, 0.2, 0.3 and 0.4) phosphors in the UV–vis range. $Y_3Al_5O_{12}$:Mn^{4+} phosphors shows obvious absorption bands in UV–vis range. There are a strong absorption band in the range of 225–400 nm and a relatively

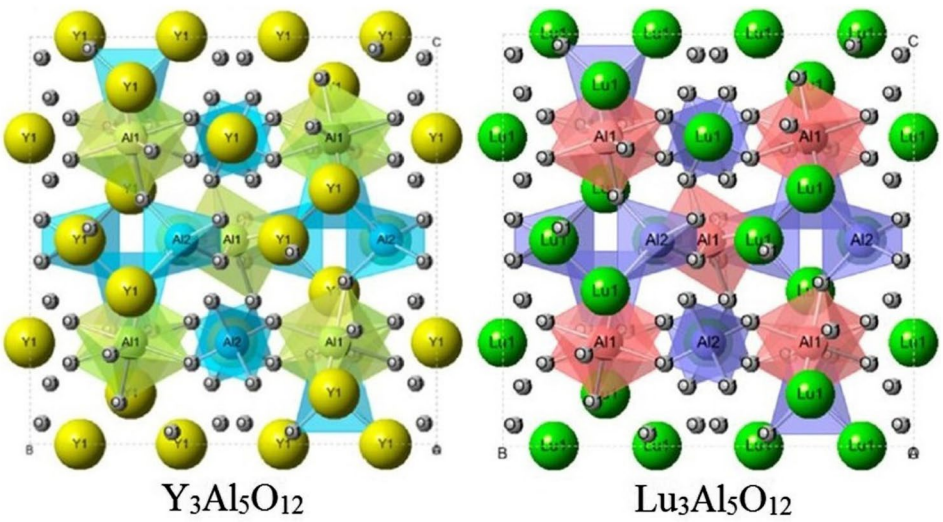

Fig. 2 Unit cell representations of $Y_3Al_5O_{12}$ and $Lu_3Al_5O_{12}$ crystal structures

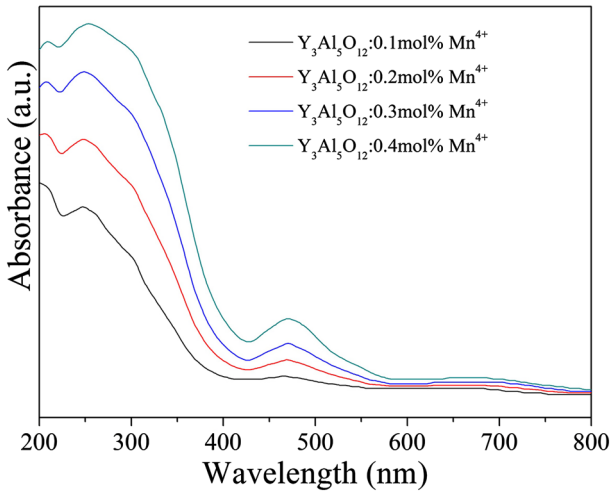

Fig. 3 Absorption spectra of $Y_3Al_5O_{12}$:x%molMn^{4+} (x = 0.1, 0.2, 0.3 and 0.4) phosphors in the UV–vis range

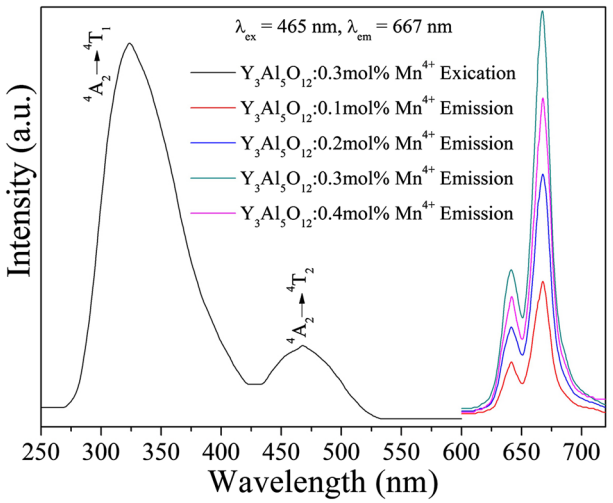

Fig. 4 Excitation spectrum of $Y_3Al_5O_{12}$:0.3mol%Mn^{4+} phosphor and emission spectra of $Y_3Al_5O_{12}$:x%molMn^{4+} (x = 0.1, 0.2, 0.3 and 0.4) phosphors

weak band in the range of 425–525 nm. The wide and strong absorption band in the range of 225–400 nm originates from the $Mn^{4+} \rightarrow O^{2-}$ charge transfer, the spin-allowed $^4A_{2g} \rightarrow {}^4T_{1g}$ and $^4A_{1g} \rightarrow {}^4T_{2g}$ transitions, but the absorption band in the range of 425–525 nm corresponds to the $^4A_{2g} \rightarrow {}^4T_{2g}$ transition [11–13]. The absorption intensity increases in UV range and the absorption edge in UV range shifts to longer wavelength with the increase of Mn^{4+} doping concentration. Unlike in UV range, the absorption intensity increases with the increasing Mn^{4+} doping concentration but the absorption edge does not vary.

Figure 4 presents the excitation spectrum of $Y_3Al_5O_{12}$:0.3mol%Mn^{4+} phosphor and emission spectra of $Y_3Al_5O_{12}$:x%molMn^{4+} (x = 0.1, 0.2, 0.3 and 0.4) phosphors. In the excitation spectrum monitored at 667 nm, there are two obvious excitation bands peaking at about 324 and 465 nm, which originates from the $^4A_{2g} \rightarrow {}^4T_{1g}$ and $^4A_{1g} \rightarrow {}^4T_{2g}$ transitions of Mn^{4+} in the octahedral coordination. The wide range of 275–525 nm for the excitation spectrum of $Y_3Al_5O_{12}$:Mn^{4+} suggests that the phosphor can be excited by the lights in UV, near-UV and blue regions. It is also worth noting that the excitation band of $Y_3Al_5O_{12}$:Mn^{4+} hardly overlaps with the emission band of $Y_3Al_5O_{12}$:Ce^{3+} (broad yellow emission band peaking at 530–540 nm) [2, 14, 15], suggesting that the risk of photon re-absorption usually taking place between the nitride red phosphor and the $Y_3Al_5O_{12}$:Ce^{3+} yellow phosphor is highly reduced. Under the excitation at 465 nm, $Y_3Al_5O_{12}$:x%molMn^{4+} (x = 0.1, 0.2, 0.3 and 0.4) phosphors show emission bands locating at deep red light region, which comes from the spin- and parity-forbidden $^2E_g \rightarrow {}^4A_{1g}$ transitions of Mn^{4+}. The emission intensity increases firstly with the increasing Mn^{4+} concentration up to x = 0.3 and then decreases with the further increasing Mn^{4+} concentration. The decrease of emission intensity is induced by the concentration quenching. Concentration quenching mechanism leads to the inability to increase the emission intensity by simply increasing Mn^{4+} ions. Moreover, it can be seen that the peaks of emission bands do not shift with the changing Mn^{4+} concentration. It is known that Mn^{4+} substitutes the site of Al^{3+} and these two ions have similar ionic radii in $Y_3Al_5O_{12}$. The similar sizes keep the lattice without any constriction or expansion. As a result, there is the invariability of the field splitting and thus the locations of emission peaks do not shift.

Figure 5 shows the emission spectra of $Y_{1-y}Lu_yAl_5O_{12}$:0.3%molMn^{4+} (y = 0, 1, 2 and 3) phosphors under the excitation at 465 nm. All of phosphors show emission bands corresponding to the spin- and parity-forbidden $^2E_g \rightarrow {}^4A_{1g}$ transitions of Mn^{4+}. The Lu^{3+} substitution does not lead to the obvious change of emission band shape but induces the slightly blue shifts of emission peaks. For $Y_3Al_5O_{12}$:0.3%molMn^{4+}, the peak of the strongest emission band locates at 667 nm. But for $Y_2LuAl_5O_{12}$:0.3%molMn^{4+}, $YLu_2Al_5O_{12}$:0.3%molMn^{4+} and $Lu_3Al_5O_{12}$:0.3%molMn^{4+} phosphors, the peaks of the strongest emission bands shift to 665, 664 and 662 nm, respectively. Generally, the Mn^{4+} luminescence has a close relation with the crystal strength and site symmetry of the host. Energy of the Mn^{4+}: $^2E_g \rightarrow {}^4A_{2g}$ transition is mainly determined by the nephelauxetic effect which is correlated with the wave-function overlap between the Mn^{4+} ions and the ligand [16–18]. As discussed above, the Lu^{3+} substitution decreases the lattice parameter and shortens the band length between Mn^{4+} and ligand O^{2-}. That is to say, Mn^{4+} experiences a stronger crystal field in $Y_{1-y}Lu_yAl_5O_{12}$:0.3%molMn^{4+} (y = 1, 2 and 3) phosphors. The stronger crystal field strength induced by

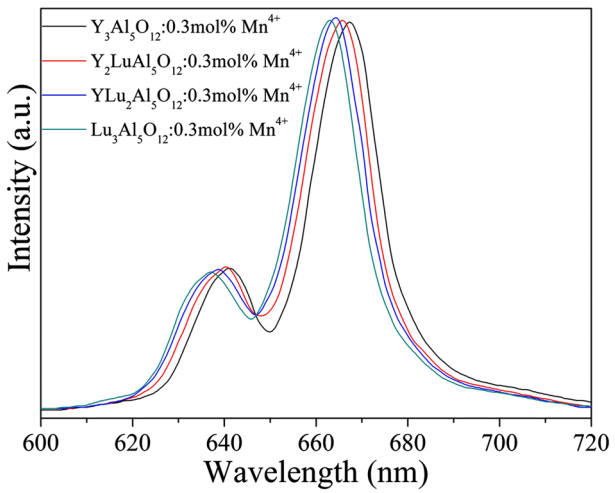

Fig. 5 Emission spectra of $Y_{1-y}Lu_yAl_5O_{12}$:0.3%molMn^{4+} (y = 0, 1, 2 and 3) phosphors

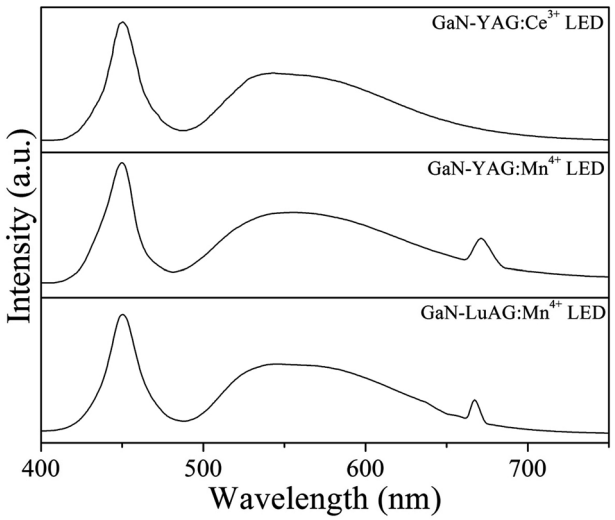

Fig. 6 Electro-luminescence spectra of the fabricated LEDs under the excitation of 20 mA current

the shorter band length between Mn^{4+} and ligand O^2 makes the energy-level splitting more, which gives rise to the blue shift of emission band for Lu^{3+} substituted $Y_3Al_5O_{12}$:Mn^{4+} phosphors.

The LEDs based on GaN blue chips were fabricated by mixing $Y_3Al_5O_{12}$:Ce^{3+} phosphor (GaN-YAG:Ce^{3+} LED) with $Y_3Al_5O_{12}$:Mn^{4+} phosphor (GaN-YAG:Mn^{4+} LED) or $Lu_3Al_5O_{12}$:Mn^{4+} phosphor (GaN-LuAG:Mn^{4+} LED). Figure 6 gives the electro-luminescence spectra of the fabricated LEDs under the excitation of 20 mA current. All of electro-luminescence spectra consist of emission bands locating at blue and yellow regions, which, respectively, originate from the blue chip and the $Y_3Al_5O_{12}$:Ce^{3+} phosphor. The emission bands locating at deep red region for GaN-YAG:Mn^{4+} and GaN-LuAG:Mn^{4+} LEDs are induced by the mixed $Y_3Al_5O_{12}$:Mn^{4+} phosphor or $Lu_3Al_5O_{12}$:Mn^{4+} phosphor. The CIE coordinates for GaN-YAG:Ce^{3+}, GaN-YAG:Mn^{4+} and GaN-LuAG:Mn^{4+} LEDs are (0.325, 0.338), (0.359, 0.327) and (0.366, 0.319), respectively. And the CCT values for GaN-YAG:Ce^{3+}, GaN-YAG:Mn^{4+} and GaN-LuAG:Mn^{4+} LEDs are 5841, 4290 and 3928, respectively. These results demonstrate that the mixed $Y_3Al_5O_{12}$:Mn^{4+} phosphor or $Lu_3Al_5O_{12}$:Mn^{4+} phosphor can decrease the CCT values of fabricated LEDs. Generally, the warm white light is suitable for home applications as the value of CCT less than 5000 K and the cold white light is suitable for commercial lighting purposes if the value of CCT higher than 5000 K [19, 20]. Therefore, we can conclude that $Y_3Al_5O_{12}$:Mn^{4+} phosphor or $Lu_3Al_5O_{12}$:Mn^{4+} phosphor is the promising commercial red phosphor in warm white LEDs.

4 Conclusion

$Y_3Al_5O_{12}$:Mn^{4+} and $Y_{1-y}Lu_yAl_5O_{12}$:Mn^{4+} phosphors were synthesized successfully by a solid state reaction. In $Y_3Al_5O_{12}$ or $Y_{1-y}Lu_yAl_5O_{12}$ hosts, Mn^{4+} ions substituted Al^{3+} sites and formed solid solutions. Under the excitation at 465 nm, the synthesized $Y_3Al_5O_{12}$:Mn^{4+} and $Y_{1-y}Lu_yAl_5O_{12}$:Mn^{4+} phosphors show emission bands corresponding to the spin- and parity-forbidden $^2E_g \rightarrow {}^4A_{1g}$ transitions of Mn^{4+}. Due to the smaller ionic radius of Lu^{3+}, the substitution of Y^{3+} by Lu^{3+} decreases the lattice parameter and thus strengthens the crystal field strength, which gives rise to the blue shift of emission band for Lu^{3+} substituted $Y_3Al_5O_{12}$:Mn^{4+} phosphors. The electro-luminescence spectra of LEDs fabricated by mixing $Y_3Al_5O_{12}$:Ce^{3+} phosphor with $Y_3Al_5O_{12}$:Mn^{4+} or $Y_{1-y}Lu_yAl_5O_{12}$:Mn^{4+} show obvious emission band locating at red region, which decreases the correlated-color-temperature of white light. $Y_3Al_5O_{12}$:Mn^{4+} and $Y_{1-y}Lu_yAl_5O_{12}$:Mn^{4+} phosphors are suitable for applications in warm white LEDs due to the compensation of red light.

Acknowledgements The work is supported by the National Natural Science Foundation of China (no. 11602066), the China Postdoctoral Science Foundation on the 56th Bath of Surface Founds the Project (no. 2014M561327), the National Science Foundation of Heilongjiang Province of China (nos. QC2015058 and 42400621-1-15047) and the Foundation Research Funds for the Central Universities (nos. HEUCF130214 and HEUCFM170204).

References

1. J.K. Sheu, S.J. Chang, C.H. Kuo, Y.K. Su, L.W. Wu, Y.C. Lin, W.C. Lai, J.M. Tsai, G.C. Chi, R.K. Wu, IEEE Photon. Technol. Lett. **15**, 18 (2003)

2. Y. Yang, J. Li, B. Liu, Y. Zhang, X. Lv, L. Wei, X. Wang, J. Xu, H. Yu, Y. Hu, H. Zhang, L. Ma, J. Wang, Chem. Phys. Lett. **685**, 89 (2017)
3. P. Pust, V. Weiler, C. Hecht, A. Tücks, A.S. Wochnik, A.K. Henb, D. Wiechert, C. Scheu, P.J. Schmidt, W. Schnick, Nat. Mater. **13**, 891 (2014)
4. G. Mo, W. Wang, K. Wang, G. Wen, M. Zhu, J. Wang, J. Mater. Sci. Mater. Electron. **28**, 8155 (2017)
5. Y. Wu, Z. Chi, T. He, J. Mater. Sci. Mater. Electron. **28**, 14591 (2017)
6. F. Baur, T. Jüstel, J. Lumin. **177**, 354 (2016)
7. B. Wang, H. Lin, F. Huang, J. Xu, H. Chen, Z. Lin, Y. Wang, Chem. Mater. **28**, 3515 (2016)
8. Y. Chen, K. Wu, J. He, Z. Tang, J. Shi, Y. Xu, Z.-Q. Liu, J. Mater. Chem. C **5**, 8828 (2017)
9. J. Long, Y. Wang, R. Ma, C. Ma, X. Yuan, Z. Wen, M. Du, Y. Cao, Inorg. Chem. **56**, 3629 (2017)
10. D. Chen, Y. Zhou, W. Xu, J. Zhong, Z. Ji, W. Xiang, J. Mater. Chem. C **4**, 1704 (2016)
11. A. Fu, L. Zhou, S. Wang, Y. Li, Dyes Pigments **148**, 9 (2018)
12. Z. Liu, H. Li, K. Liu, H. Yu, K. Cheng, Sol. Energy **142**, 61 (2017)
13. J. Liu, Y. Li, J. Ke, S. Wang, L. Wang, H. Xiao, Appl. Catal. B Environ. **224**, 705 (2018)
14. Y. Kim, K.B. Shim, M. Wu, H.-K. Jung, J. Alloys Compd. **693**, 40 (2017)
15. W.T. Hong, J.H. Lee, J.W. Son, Z. Lee, H.J. Park, H.S. Kim, J.S. Lee, H.K. Yang, Ceram. Int. **42**, 2204 (2016)
16. M.G. Brik, S.J. Camardello, A.M. Srivastava, ECS J. Solid State Sci. Technol. **4**, R39 (2015)
17. M.G. Brik, A.M. Srivastava, ECS J. Solid State Sci. Technol. **2**, R148 (2013)
18. Z. Liu, H. Li, G. Cao, Int. J. Environ. Res. Public Health **14**, 857 (2017)
19. Z. Liu, W. Xu, X. Zhai, C. Qian, X. Chen, Renew. Energy **101**, 1131 (2017)
20. V. Neharika, J. Kumar, V.K. Sharma, O.M. Singh, H.C. Ntwaeaborwa, Swart, J. Electron. Spectrosc. **206**, 52 (2016)